

# Effect of pH and hydration on the normal and lateral interaction forces between alumina surfaces

M. Polat<sup>a,b,\*</sup>, K. Sato<sup>b</sup>, T. Nagaoka<sup>b</sup>, K. Watari<sup>b</sup>

<sup>a</sup> *Izmir Institute of Technology, Department of Chemical Engineering, Urla Izmir, Turkey*

<sup>b</sup> *National Institute of Advanced Industrial Science and Technology (AIST), Advanced Sintering Technology Group, 463-8560 Nagoya, Aichi, Japan*

Received 4 July 2006; accepted 30 August 2006

Available online 11 October 2006

## Abstract

Interaction forces between alumina surfaces were measured using an AFM–colloid probe method at different pHs. For an  $\alpha$ -alumina–sapphire system at acidic pH, the force curve exhibited a well-defined repulsive barrier and an attractive minimum. At basic pH, the interactive force was repulsive at all separations with no primary minimum. Lateral force measurements under the same conditions showed that frictional forces were nearly an order of magnitude smaller at basic pH than those observed at acidic pH. This behavior was attributed to the hydration of the alumina surface. Normal and lateral force measurements with the strongly hydrated  $\rho$ -alumina surfaces supported these findings.

© 2006 Elsevier Inc. All rights reserved.

**Keywords:** Atomic force microscopy; Colloid probe; Force curve; DLVO theory

## 1. Introduction

Interaction forces between colloidal particles play an important role in numerous physicochemical systems in mineral, ceramic, and environmental sciences since they determine stability, rheology, and forming characteristics. Hence, careful analysis of these forces is of the utmost practical importance in predicting and controlling the behavior of these systems.

Direct measurement of interparticle forces has been possible with the introduction of the surface force apparatus (SFA) [1–5]. However, the SFA can only be used with transparent substrates and lacks lateral resolution [6]. The atomic force microscope (AFM), which is not hampered by such shortcomings, has been finding wider use for in situ measurements of the interactive forces in a variety of systems. In an AFM force measurement, a cantilever a few hundred micrometers long equipped with a tiny tip on the free end is progressively approached to a surface. The cantilever bends by a finite amount due to the action of electrostatic and interatomic forces. The amount of bending, which depends strongly on the distance be-

tween the tip and the surface, can be measured quantitatively by a laser–photodetector system and related to the interactive force through the spring constant of the cantilever. If a colloidal particle is attached to the cantilever, the measured forces are those acting between this particle and the substrate. The technique is called the colloid probe method [7–9]. Since quantum-level resolutions are possible with the AFM [10], forces on the order of few picoNewtons can theoretically be detected. Due to this power in resolution and its flexibility, a large volume of work with the AFM–colloid probe method has appeared in the literature in the past decade. The reader is directed to the original work by Ducker et al. [7–9] and excellent reviews by Parker [11], Claesson et al. [12], Senden [13], and Hodges [14].

DLVO theory states that the net energy of interaction between two surfaces dispersed in a liquid medium is the sum of electrical double layer and van der Waals forces [15,16]. The van der Waals force is mainly affected by the bulk properties of the interacting bodies and the separating medium. The electrostatic force is influenced by the surface properties, and hence by the solution chemistry, since it owes its presence to the spontaneous formation of an electrical double layer due to different chemical activities of ions on the surface and in solution.

\* Corresponding author. Fax: +90 232 750 6645.

E-mail address: [mehmetpolat@iyte.edu.tr](mailto:mehmetpolat@iyte.edu.tr) (M. Polat).

In the case of metal oxides such as alumina, protons are the main ionic species responsible for altering the charging characteristics of the surface. Direct force measurements with SFA and AFM have shown that, under certain conditions, metal oxide–water interfaces may display an unusual behavior that cannot be accounted for by the DLVO theory, especially at short distances of separation [17–23].<sup>1</sup> One of the explanations of such behavior was to invoke a repulsive “hydration force” at separations shorter than 5 nm. However, debate on the basis of such behavior and its eventual effect on the system is still continuing.

In this study, systematic measurements of the normal and lateral interaction forces between  $\alpha$ - and  $\rho$ -alumina colloid probes and a sapphire substrate were carried out using the AFM–colloid probe method as a function of pH and compared with the theory in order to illustrate how these forces vary with the pH and to determine the underlying reasons for such behavior.

## 2. Materials and methods

An  $\alpha$ -alumina powder (AO-802 from Admatechs Co., Japan) consisting of spherical particles (mean size 9.9  $\mu\text{m}$ ) was used for the preparation of the  $\alpha$ -alumina colloid probes and for the zeta potential measurements. A much finer size fraction of the same powder (mean size 0.7  $\mu\text{m}$ ) was employed for the FTIR–DRIFT and TG–DTGA studies.

A  $\rho$ -alumina powder (BK-105, Sumimoto Chemical Co., Ltd., Japan) consisting of irregular-shaped rounded particles (mean size 5  $\mu\text{m}$ ) was used for the preparation of the  $\rho$ -alumina colloid probes and for the zeta potential measurements. The XRD measurements carried out previously demonstrated that this sample hydrated strongly if it was aged in pH 9 solutions for about 4 days [26]. It was shown that the dominant initial  $\rho$ -alumina phase transformed progressively into a bayerite ( $\text{Al}_2\text{O}_3 \cdot 3\text{H}_2\text{O}$ ) and boehmite ( $\text{Al}_2\text{O}_3 \cdot 1-2\text{H}_2\text{O}$ ) gel.

A sapphire sample with a 0001 orientation (1  $\times$  1 cm flat substrate coded SA100510, As One Corporation, Japan) was used as the substrate in all tests. The sample was atomically smooth with a surface average roughness of 0.05 nm with the largest peak-to-valley distance about 0.109 nm, as determined by the AFM scans.

Tipples rectangular cantilevers (TL-FM-50, Nanosensors, Switzerland) employed in the study were packed in batches of 50. The cantilevers in each batch was reported by the manufacturer to have lengths between 215 and 235  $\mu\text{m}$ , widths between 21.5 and 35.5  $\mu\text{m}$ , resonant frequencies between 45 and 115 kHz, and force constants between 0.5 and 9.5 N/m.

The glue utilized to fix the colloid probe onto the cantilever was a rapid-type epoxy glue (Araldite AR-R30, Nichiban Co. Ltd., Japan).

All the solutions were prepared from double-distilled water (Yamato Scientific Auto Still Model WA-72, Japan) that was passed through a reverse-osmosis unit (Barnstead/Thermolyne

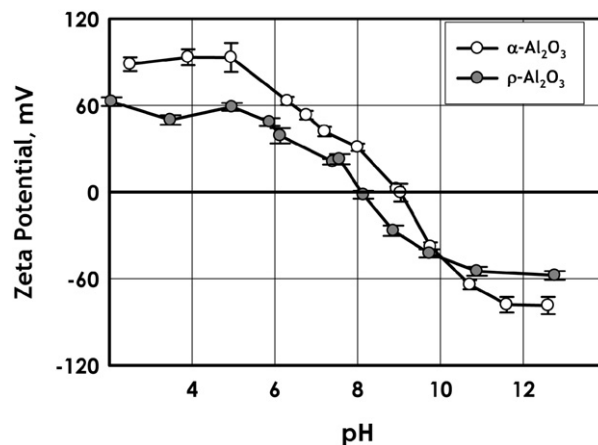


Fig. 1. Zeta potential of the  $\alpha$ - and  $\rho$ -alumina powders used in preparing the colloid probes (in  $10^{-2}$  M KCl solutions). The error bars are the 95% confidence intervals for a repeat of six zeta potential readings.

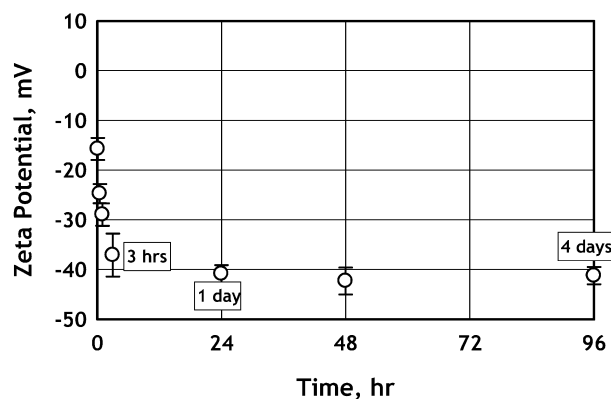


Fig. 2. Effect of aging on the zeta potential of the  $\rho$ -alumina sample.

EasyPure, USA). The resulting water was reagent grade water with extremely low organic carbon content and had a minimum resistance of 18.3 M $\Omega$  cm. Polyethylene bottles were used to prepare the solutions throughout the work. Ethanol used in the tests was pure reagent grade.

Zeta potential measurements with fresh  $\alpha$ - and  $\rho$ -alumina powders were obtained in 0.01 M KCl solutions at a solid/liquid ratio of 0.1 g/L within 30 min of contact with solution. Results are presented in Fig. 1. Each zeta potential was an average of 6 readings and was periodically checked against the standard solution. It can be seen that the higher iep of the  $\alpha$ -alumina (at around pH 9.1) suggests a surface slightly more basic than that of  $\rho$ -alumina (at around pH 8.1). The results of the zeta potential measurements where the  $\rho$ -alumina sample was aged in pH 9/0.01 M KCl solutions up to 4 days are presented in Fig. 2. It can be seen that the zeta potential of the  $\rho$ -alumina sample shows a decline from about  $-15$  to  $-40$  mV within the first 3 h but remains nearly constant afterward. No zeta potential measurements were carried out with the sapphire sample since AFM and streaming potential data for sapphire were available in the literature, indicating an iep between 5.0 and 6.0 for different orientations [27]. The comparatively lower iep of the sapphire was attributed to the attachment of the surface OH groups to multiple Al atoms.

<sup>1</sup> In addition to this short-range force, several works suggest the presence of a so-called long-range (>100 nm) attractive interaction for hydrophobic surfaces [9,24,25].

Since a  $\rho$ -alumina sample was found to hydrate strongly in a previous paper [26], FTIR-DRIFT (Perkin–Elmer Spectrum GX FTIR System with DRIFT), and TG-DTA (Model 2000S from Mac Sciences Co. Ltd., Japan) studies were carried out with the  $\alpha$ -alumina sample only. The  $\alpha$ -alumina powder with mean particle size 0.7  $\mu\text{m}$  was utilized for the purpose. In these tests, 5 g  $\alpha$ -alumina powder was dispersed in 100 ml of a solution of  $10^{-4}$  M KCl at two different pH values, 3.5 and 12. The dispersion was kept in a shaker for 24 h, filtered, vacuum-dried at room temperature, and subjected to FTIR-DRIFT and TG-DTA measurements.

### 3. Procedure employed in obtaining the force curves and comparing them with the theory

#### 3.1. Calibration of the cantilevers and spring constant determination

Each tipless cantilever in a batch of 50 was individually tested for its dimensions, resonant frequency, and Q factor at room temperature to determine the normal spring constant using Sader's formula. The procedure is described in the literature in detail [28–30]. The spring constants for the unloaded cantilevers were reported to be valid for the colloid probe systems. The spring constants measured for the batch varied between 2.1 and 4.0 N/m with a mean value of 3.1 N/m. The tested cantilevers were always stored in an evacuated container until use.

Determination of the lateral spring constants was not attempted in this work due to the presence of several components with indeterminable properties in the colloid probe system (the colloid particle, the glue joint, and the cantilever). Though they have a minimal effect on the normal spring constant [28–30], these complications decrease the reliability of the lateral spring constant determination. Nevertheless, the torsional angle of the cantilever, which is directly related to the signal obtained from the AFM, is actually equal to the frictional force divided by the lateral spring constant and can be treated as a dimensionless frictional force. Provided that the same colloid probe is used for a given set of tests, use of the dimensionless frictional force should be valid for comparing the lateral force results.

#### 3.2. Colloid probe preparation

A challenging part of the work was to classify the powders into a narrow size range (5–10  $\mu\text{m}$  range) and to en-

sure that the surfaces of these particles did not contain any nanosized secondary particles. A repeated chemical dispersion/ultrasonification/decantation procedure was employed to single out and clean the bulk alumina particles to be used as colloid probes. A quantity of 0.1 g of alumina powder was dispersed in a 100-ml solution in a 10-cm-long phial and subjected to ultrasonic treatment for 10 min. The solutions used for the purpose was sodiumhexametaphosphate solution at pH 3.5 for  $\alpha$ -alumina and ethanol solution for  $\rho$ -alumina. The dispersion was rested for a specific time calculated by the Stokes equation to settle out the particles of a desired size range. The upper part of the solution in the phial was vacuumed out using a burette while the lowermost 1 cm was kept undisturbed. The phial was completed to 100 ml with the same solution and the whole process was repeated five times. The final product was a dispersion containing particles between 5 and 10  $\mu\text{m}$ . These particles were stored in ethanol until use. To place the colloid probe particles on the cantilevers, a fraction of this stock solution was filtered from a membrane filter after dilution and dried in a vacuum desiccator.

Some representative SEM photographs of the  $\alpha$ -alumina particles prepared using the above procedure are presented in Fig. 3. Fig. 3a demonstrates clearly the problem of unwanted nanosized particles on an  $\alpha$ -alumina particle obtained after insufficient preparation (a single decantation in distilled water). Note the flattened points of contact between the secondary particles and the mother particle, which plainly illustrate the strength of the colloidal forces in question. A representative photo of a clean  $\alpha$ -alumina particle after sufficient preparation (five times decantation in pH 3.5 Calgon solution aided by ultrasonification) is presented in Fig. 3b. The photo in Fig. 3c demonstrates that the surface of the alumina particle is quite smooth down to a few nanometers.

A micromanipulator (Model M501-1202-M, Suruga Seiki Co. Ltd., Japan) with submicrometer resolution and coupled to a long-range microscope-image processing unit (magnification  $\times 2800$ ) was employed to manipulate and glue the colloid probe particles on the cantilevers. The manipulator possessed two arms having X–Y–Z translational freedom with submicrometer resolution. The arms were situated on a stage having X–Y translational freedom, again with sub-micrometer resolution. A 5- $\mu\text{m}$  capillary connected to a microvolume vacuum pump was attached onto one arm and employed to pick the particles. A rod with a tip diameter of 2  $\mu\text{m}$  was attached to the

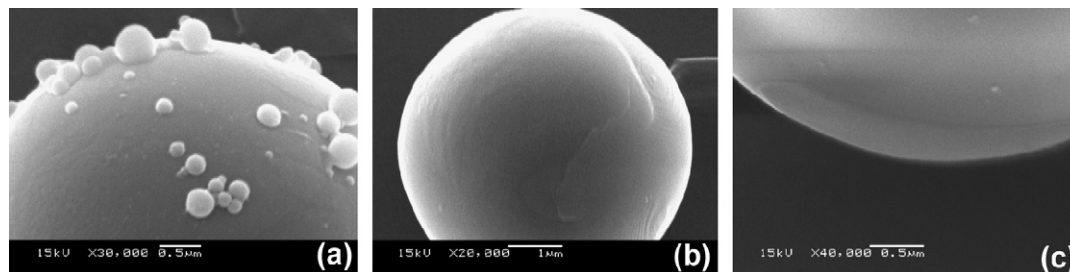


Fig. 3. Some illustrative pictures of the  $\alpha$ -alumina colloid probes: (a) a representative particle from a solution decanted once in distilled water without ultrasonic treatment, (b) a representative particle from a solution ultrasonified/decanted five consecutive times in pH 3.5 Calgon solution, and (c) a close-up view of the surface of a clean probe particle.

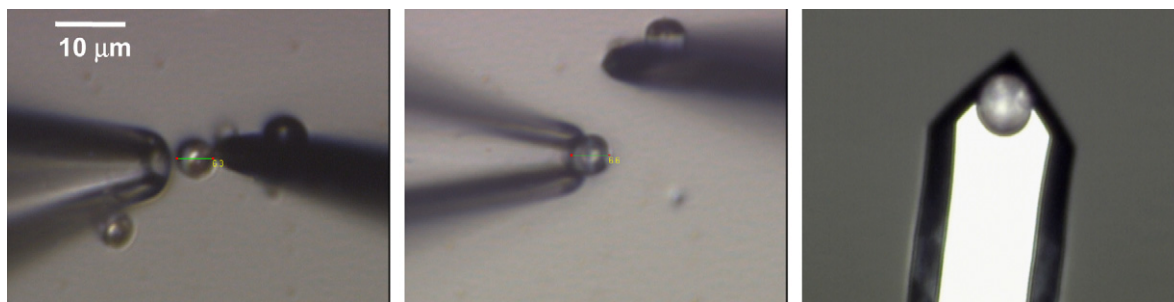


Fig. 4. Manipulation of the colloid probes with the micromanipulator system and a colloid probe particle placed on a rectangular cantilever (the scale applies to all three photos).

other arm and utilized to apply the glue and align the particles on the cantilever. Some illustrative pictures of the  $\alpha$ -alumina particles being manipulated are presented in Fig. 4. Since the particles of the  $\rho$ -alumina powder were not perfect spheres, special care had to be taken to isolate rounded  $\rho$ -alumina particles with well-defined apexes to prepare the colloid probes. In this case, the same probe particle was used for a given set of experiments to avoid geometrical deviations of the colloid probe particles.

### 3.3. Treatment of the surfaces

The sapphire, the colloid probe, and the liquid cell were all subjected to UV treatment for 10 min (Photo Surface Processor, Model PL16-110D, Sen Light Corp., Japan) before each test. They were then washed with ethanol, water, and experimental solution used copiously. The sapphire and the colloid probe were placed in the quartz cell containing the experimental solution 10 min before the force measurements. The total time the particles remained in the cell was around 30 min in a typical test. In the tests where the  $\rho$ -alumina probes were aged to vary the degree of hydration, the whole assembly was kept in a pH 9 solution for up to 4 days and the pH was adjusted periodically, while the force measurements were carried out at predetermined intervals.

The micromanipulator system was also used to carry out micro-contact-angle measurements [31] on the treated sapphire surface, using the captive bubble method to determine the surface cleanliness. No bubble attachment was observed, indicating that the treated sapphire surface was perfectly clean and hydrophilic.

Use of a quartz cell in the force measurements raises the possibility of silica contamination. The primary dissolved silica species in basic solutions are the negatively charged, cascading  $\text{H}_2\text{SiO}_4^{2-}$  (pH > 9),  $\text{HSiO}_4^{3-}$  (pH > 10), and  $\text{SiO}_4^{4-}$  (pH > 11) ions. The results of Löbbus et al. [32] show that at a pH of about 9.5, the highest dissolved silica concentration observed after 4 weeks is about 2.5 nmol/L in solutions of 0.01 M NaCl containing 46 m<sup>2</sup> amorphous glass surface per liter of test solution. Assuming an approximate parking area of 20 Å<sup>2</sup>, this amount of dissolution would correspond to a coverage of about 0.3% of the sapphire substrate used despite the much smaller silica/liquid contact area (0.36 m<sup>2</sup> per liter) and much shorter contact times employed in our tests. The recent study by Wolff–

Boenisch [33] shows that though the silica dissolution from several glasses at pH 10.6 is about five times higher than that observed at pH 4.0, the dissolution was strongly affected by the surface area of the glass spheres. Furlong et al. [34] states explicitly that the silica adsorption on single alumina crystals is only possible at “extensive aging times.” This is probably the reason behind the finding of Franks and Meagher [27], who used XPS analysis to completely rule out silica contamination from the glass cell in their AFM work at a basic pH. The excellent reproducibility of the multiple force measurements obtained on different locations on the sapphire substrate (both at acidic and basic pH) also suggests a uniform surface state in our tests.

### 3.4. Acquisition of normal and lateral force data

A scanning probe microscope (SPA 400 with SI3800 Probe Station, Seiko, Japan) equipped with a proper cantilever holder suitable for in-liquid measurements was employed for the normal and lateral force measurements. The substrate–colloid probe contacts were achieved in a circular quartz cell (25.0 mm in diameter and 5 mm in height) filled with the appropriate experimental solution.

In this specific AFM, only the piezo that holds the sapphire sample has vertical traversing capability. The colloid probe’s vertical motion can take place only if there is any bending of the cantilever. For example, assuming two noninteracting surfaces, a displacement of the piezo ( $D$ ) by 10 nm means the same amount of decrease in the gap separating the surfaces ( $h$ ) when they are far apart. However, if the surfaces are separated by a distance, say,  $h = 6$  nm, to begin with, a vertical movement of the piezo by  $D = 10$  nm results in contact after the first 6 nm. When the piezo’s 10-nm translation is completed, the cantilever will show vertical bending of  $x = 4$  nm. This simply means that a vertical piezo displacement of 100 nm does not always mean the same amount of change in the separating gap. Rather, this amount will correspond to the sum of the change in the separating gap and the vertical bending of the cantilever.

The force measurements were carried out at five different points on a  $5 \times 5 \mu\text{m}$  section of the sapphire surface (at the corners 500 nm from each side and at the center). The same procedure was repeated on several different sections on the sapphire surface to check reproducibility, which was observed to be excellent. In the normal force measurements, the sapphire sur-

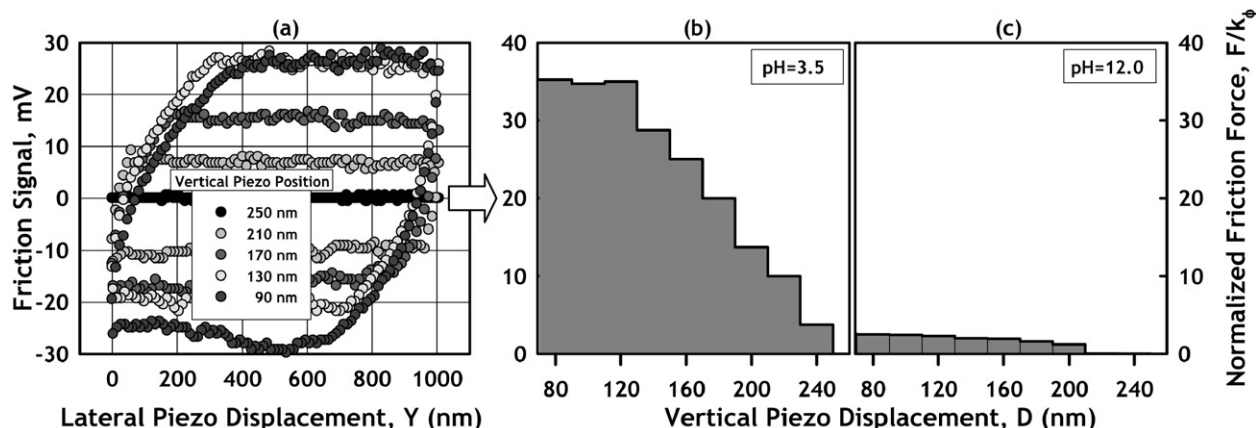


Fig. 6. Raw friction data (a) and dimensionless friction forces (b and c) for the interaction of  $\alpha$ -alumina colloid and sapphire substrate. Experimental conditions:  $C_0 = 10^{-4}$  M KCl,  $T = 25^\circ\text{C}$ ,  $R = 5.4 \mu\text{m}$ ,  $k_n = 3.1 \text{ N/m}$ .

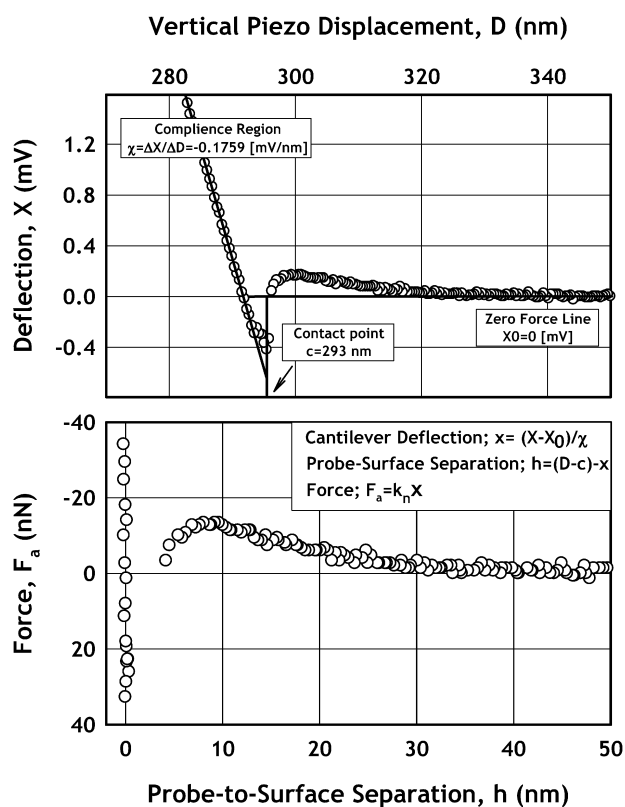


Fig. 5. An example of raw force curve data (average of five separate readings) obtained with an  $\alpha$ -alumina colloid probe and sapphire substrate at pH 3 (top figure) and the final resulting force curve (bottom figure).  $R$  is the particle radius and  $k_n$  is the normal spring constant.

face (piezo) was approached and detracted at a constant speed of  $30 \text{ nm/s}$  in all cases. The five raw force curve readings obtained for a given test were used to calculate an average force curve for that test. The procedure is illustrated in Fig. 5 and the algorithm used for raw force signal to actual force curve conversion can be seen in the inset box given in the bottom graph.

The frictional force measurements were carried out immediately after the normal force measurements over the same points on the sapphire surface by the relative lateral displacement of the colloid probe on the sapphire surface ( $Y$ ). The amplitude

and the speed of the lateral scan were  $1 \mu\text{m}$  and  $1 \mu\text{m/s}$ , respectively. To eliminate the unavoidable effect of different probe-to-surface separations on frictional force, 10 lateral scans were obtained at selected probe-to-surface separations by step-wise approaching (or pushing) the sapphire substrate to the colloid probe (Fig. 6a). The scans in this figure were normalized around zero using the built-in normalization algorithm of the AFM software, which resulted in positive signals for the forward scan and negative signals for the reverse scan.

In a given set of lateral tests, the probe was taken to an arbitrarily far distance from the surface and a lateral scan was made. In this case, naturally there was no friction and a flat zero line was observed. The process was repeated by gradually approaching the substrate to the probe until the first nonzero friction signal was obtained. These data were saved as the first friction data set and 10 lateral scans were obtained by progressively moving the piezo toward the surface, which gave increasingly larger friction signals (see Fig. 6a, which shows 5 of these scans). Then using a representation based on the effect of change of vertical piezo displacement  $D$  on the frictional force allows us to compare the relative frictional behavior of the two cases after the first signs of friction were obtained.

An equilibrium dimensionless frictional force versus probe-to-surface distance curve could be obtained from the lateral scans obtained at each piezo displacement (see Fig. 6b). The equilibrium dimensionless frictional force is obtained by dividing the equilibrium friction signal (the region where the frictional signal attains a constant magnitude on the surface during lateral scan) by the slope of the initial part of the scan (the initial region where the signal is increasing in magnitude from zero to the equilibrium value). The reasons for the use of a dimensionless frictional force representation were explained in Section 3.1 previously.

### 3.5. Calculation of the theoretical curves

The theoretical force calculations were carried out based on the DLVO theory, assuming that the net force of interaction ( $F_{\text{net}}$ ) per unit area of the interacting plates was a sum of van der Waals and double-layer forces. The force per area on any

one of the plates (pressure force) due to the van der Waals component ( $F_{vdW}$ ) is equal to

$$F_{vdW} = -\frac{A}{6\pi h^3}, \quad (1)$$

where  $A$  is the Hamaker constant and  $h$  is the interplate separation. This equation assumes that the van der Waals interaction is in the nonretarded region, which is not a bad assumption, since the measured forces were mainly significant below about 10 nm. The Hamaker constant for alumina surfaces interacting in water was taken as  $A_{awa} = 4.8 \times 10^{-20}$  J, an average of several values reported in Refs. [35–38].

For calculating the electrostatic pressure force ( $F_{el}$ ), a full numerical solution of the Poisson–Boltzmann equation,

$$\frac{d^2\psi}{dx^2} = \frac{\kappa^2 RT}{zF} \sinh\left(\frac{zF\psi}{RT}\right), \quad (2)$$

was obtained by numerical shooting procedures assuming a symmetrical electrolyte solution (see Appendix A for the core shooting procedure algorithm for the potential profile between the two surfaces). Here,  $\psi$  is the potential at any point  $x$  between the plates separated by a gap  $h$ ,  $C_0$  is the electrolyte concentration in the solution,  $R$  is the gas constant,  $T$  is the temperature, and  $z$  is the ionic valence. The surface charge and surface potential at each separation  $h$  can simultaneously be determined from these potential profiles computed for each  $h$ . The electrostatic force per unit area can be calculated using

$$F_{el} = 2C_0RT \left[ \cosh\left(\frac{zF\psi_0}{RT}\right) - 1 \right] - \frac{\varepsilon\varepsilon_0}{2}\sigma_0^2, \quad (3)$$

where  $\sigma_0$  is the surface charge on any one of the plates with surface potential  $\psi_0$  at separation  $h$  and  $\varepsilon_0$  and  $\varepsilon$  are the permittivity of the vacuum and the relative permittivity of water, respectively.

Since the real system is a flat surface (sapphire) interacting with a spherical particle (colloid probe), the force measured has units of nanoNewtons. Since the above formulae give the force per unit area for two plates, a transformation between the two is required. Though more elaborate techniques are available [39,40], Derjaguin's approach can safely be employed to normalize the force calculations. Separation distances shorter than 100 nm and colloid probe diameters of about 10  $\mu\text{m}$  correspond to an  $h/2R$  value smaller than 0.01. This value is well within the range of Derjaguin's approximation [6,39]. Then, based on Derjaguin's approximation, the actual force of interaction in units of newtons ( $F_a$ ) is equal to  $F_{net}$  as follows:

$$F_a = 2\pi R \int_h^\infty F_{net}(h) dh. \quad (4)$$

The numerical calculation of the double layer forces was carried out both for constant-potential and constant-charge surfaces. These two cases essentially define two boundaries for possible charging conditions. The potentials employed in these calculations were estimated from the zeta potential measurements given in Fig. 1 for the  $\alpha$ -alumina probes and from the literature [27] for the sapphire substrate. The respective values

were 90/70 for pH 3.5, 40/–40 for pH 7.7, and –80/–60 for pH 12. The electrolyte strengths used for computing the theoretical curves were  $10^{-4}$  M for pH 3.5 and 7.7 and  $10^{-2}$  M for pH 12 due to high ionic strength at this basic pH.

#### 4. Results and discussion

The results of the normal force measurements with an  $\alpha$ -alumina probe are given in Fig. 7 as a function of separation for pH values of 3.5, 7.7, and 12 (circles). The reason for choosing these specific pH values is as follows: at pH 3.5, both the sapphire and the  $\alpha$ -alumina should be positively charged, since pH 3 is below the iep of both solids. Conversely, both surfaces must be negatively charged at pH 12. The surface charge at pH 7.7 should be negative for sapphire and positive for the  $\alpha$ -alumina colloid probe. Therefore, besides the attractive van der Waals forces, the surfaces should feel an electrostatic re-

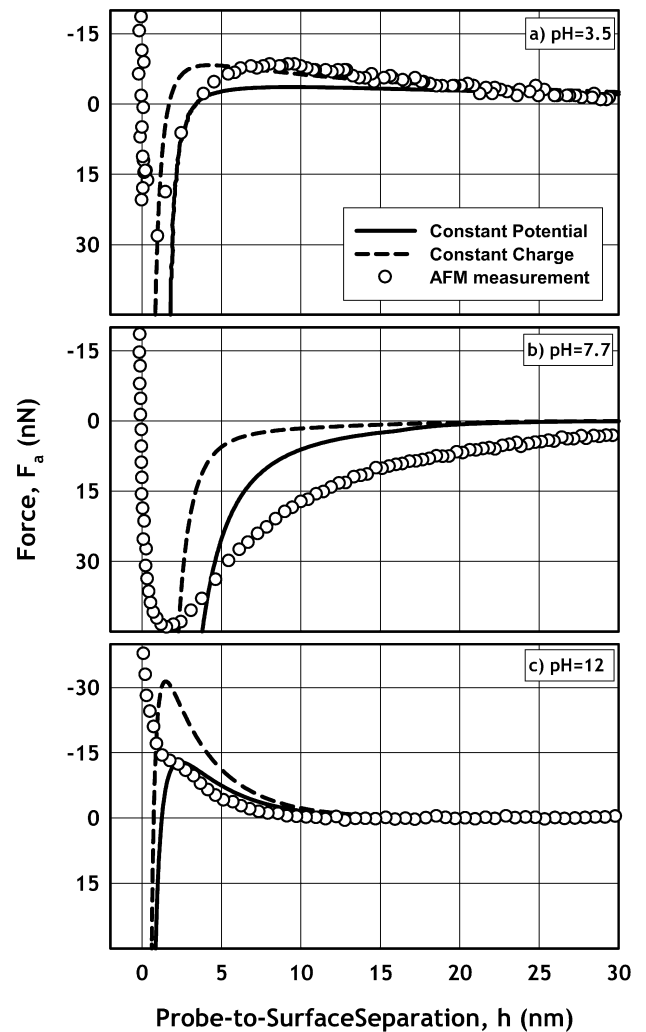


Fig. 7. Effect of solution pH on the measured and theoretical interaction forces between  $\alpha$ -alumina colloid probe and sapphire substrate. Constant potential and constant charge lines were drawn using 90/70 mV for pH 3.5, 40/–40 mV for pH 7.7, and –80/–60 mV for pH 12. Electrolyte strength was set to be  $10^{-4}$  M for pH 3.5 and 7.7 and  $10^{-2}$  M for pH 12 (due to high ionic strength at pH 12  $A_{awa} = 4.8 \times 10^{-20}$  J. Experimental conditions:  $C_0 = 10^{-4}$  M KCl,  $T = 25^\circ\text{C}$ ,  $R = 5.4 \mu\text{m}$ ,  $k_n = 3.1$  N/m.

pulsion at pH values of 3.5 and 12, whereas the electrostatic component should also be attractive at pH 7.7. The theoretical force curves computed as explained in Section 3.5 are also presented in Fig. 7. The solid and dashed lines represent the constant-potential and constant-charge scenarios, respectively. The parameters employed in computing these curves are given below the figure title.

The measured force data presented in Fig. 7 display major differences as a function of pH. For the pH 3.5 case (Fig. 7a), a repulsive barrier can be clearly seen with a maximum at around 10 nm. At closer approach, the force of interaction becomes attractive very quickly and a primary minimum develops before the colloid probe and the sapphire surface come into contact. It is clearly seen that both the data and the theoretical curves display an energy barrier followed by a primary minimum. Since the measured forces nicely fall within the theoretical constant-potential and constant-charge lines, it can be said that aluminum oxide surfaces interact mainly through van der Waals and electrostatic interactions under acidic conditions.

The middle graph in Fig. 7 presents the forces measured at pH 7.7. Not surprisingly, the interaction is attractive irrespective of separation at this pH, since the two surfaces are charged oppositely. The DLVO theory seems to predict smaller attractive forces, but again the general trend followed by both the measured data and the theoretical curves is similar.

The bottom graph in Fig. 7 gives the interaction force at pH 12. It is immediately apparent that, similarly to Fig. 7a, the data and the theory agree quite well until a separation of a few nanometers. However, at very close separations, the measured data and the theory disagree not only quantitatively, but also in a qualitative manner. The measured force curve does not show any distinct repulsive barrier nor a primary minimum. It is always repulsive at very close separations, while the theoretical curves still predict a primary minimum at close range. Such a lack of primary minimum at close separation is an indication that another factor besides the van der Waals and electrostatic forces is playing a role in the system when they approach closer than 5 nm. Other evidence of such repulsion was observed in the literature and attributed to the possibility of surface hydration, as was already discussed in the Introduction.

Fig. 6 gives the results of the lateral force measurements obtained at the same points where the normal force measurements were obtained for the pH 3.5 and 12 cases. Fig. 6a gives the selected lateral scans for illustrative purposes at different vertical piezo positions ( $D$ ) for the pH 3.5 case. It can be seen that the friction signal increases significantly as the piezo approaches the surface progressively, as expected. Figs. 6b and 6c give the average dimensionless frictional force as a function of vertical piezo displacement for the pH 3.5 and 12 cases, respectively. The results in the figure demonstrate a very important feature of the system, that the frictional forces are an order of magnitude smaller at basic pH. The fact that the normal forces were repulsive at this pH due to probable hydration implies that the hydration water prevents the closer approach of the two surfaces and acts as a medium over which the surfaces slide over each other more easily. It is conjectured that at this point the presence of water that is strongly attached to the hydrated surface

may be acting some kind of lubricant, decreasing the frictional forces. However, the source of this friction can be the subject of a more comprehensive study in this direction. Such a study should also pay attention to the effect of hydrodynamic factors on the magnitude of frictional forces.

To see the effect of hydration more clearly, similar experiments were carried out using  $\rho$ -alumina colloid probes. The  $\rho$ -alumina was previously shown to be completely hydrated to a gel within 4 days (see Section 2 and Ref. [26]). Hence, the  $\rho$ -alumina colloid probes were aged in pH 9 solutions for up to 4 days to change the degree of hydration, while force measurements were carried out periodically. The reason for the selection of pH 9 was to work at the natural pH of the  $\rho$ -alumina slurries and to minimize the effect of electrostatic component. The results of the normal and lateral force measurements are presented in Figs. 8 and 9, respectively, for 3 h, 1 day, and 4 days of aging. The zeta potential measurements carried out with the  $\rho$ -alumina slurries under the same conditions that were previously presented in Fig. 2 show that the potential on the surface stabilizes after 3 h and remains nearly constant around  $-40$  mV. The normal force measurements given in Fig. 8 show that there is a clear attraction between the two surfaces initially. Though both surfaces should be predominantly negatively charged, it is apparent that the van der Waals component is dominating. Nevertheless, the attraction is about four times smaller than that observed with the  $\alpha$ -alumina probes at pH 7.7, where the surfaces were oppositely charged. The amount of attraction decreases, however, with time of aging of the  $\rho$ -alumina sample. After 4 days, the interaction is decidedly repulsive. The lateral force measurements carried out on the same points (Fig. 9) show clearly that the frictional forces decrease precipitously with the aging of the  $\rho$ -alumina.

However, on the whole, these results conclusively indicate that hydration of the aluminum oxide surfaces not only leads to measurable repulsion between the two surfaces, but also decreases the frictional forces. They also show clearly that, because of this repulsion, the DLVO theory, which represents the oxide interactions extremely well at acidic pH values, fails completely at basic pH values.

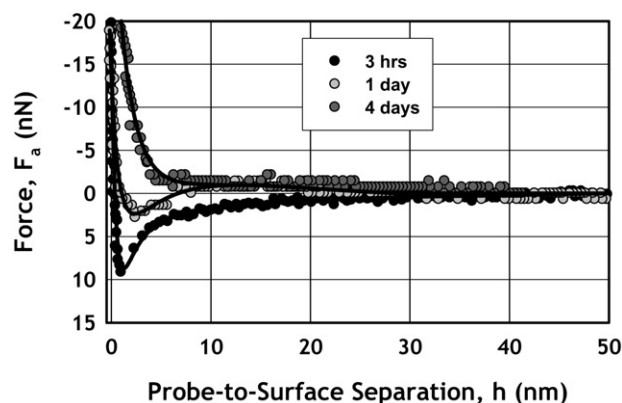


Fig. 8. Effect of aging of the  $\rho$ -alumina sample on the normal interaction forces between the  $\rho$ -alumina colloid probe and the sapphire substrate. The solid lines are drawn to guide the eye. Experimental conditions: pH 9,  $C_0 = 10^{-4}$  M KCl,  $T = 25^\circ\text{C}$ ,  $k_n = 3.0$  N/m,  $R = 6.2$   $\mu\text{m}$ .

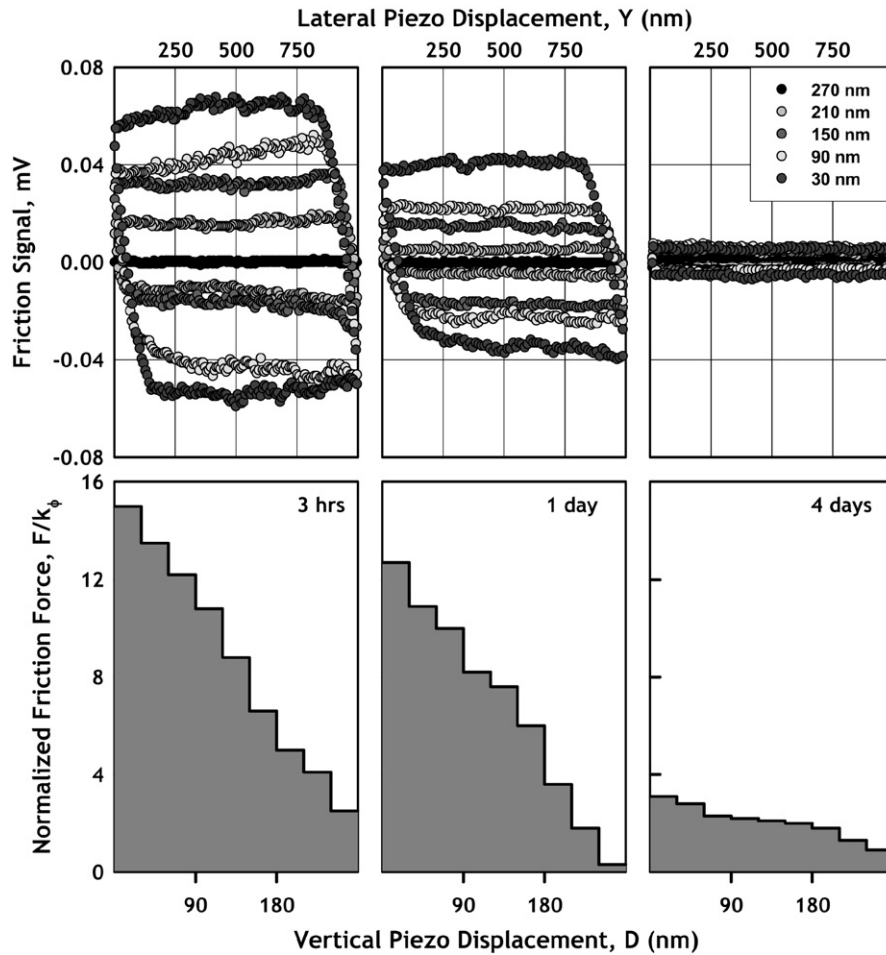


Fig. 9. Effect of aging of the  $\alpha$ -alumina sample on the lateral interaction forces between the  $\alpha$ -alumina colloid probe and the sapphire substrate. Experimental conditions: pH 9,  $C_0 = 10^{-4}$  M KCl,  $T = 25^\circ\text{C}$ ,  $k_n = 3.0$  N/m,  $R = 6.2$   $\mu\text{m}$ .

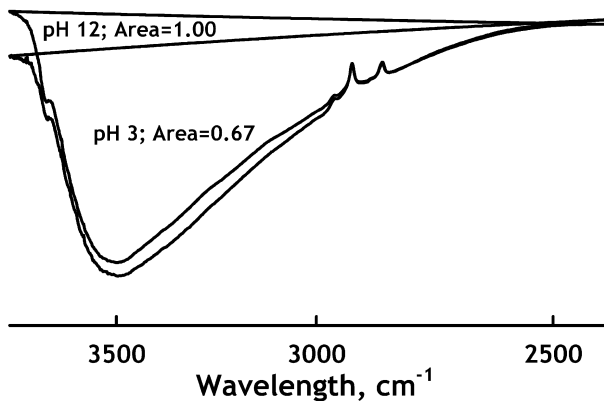


Fig. 10. FTIR-DRIFT normalized spectra of the H-bonded water region for the  $\alpha$ -alumina samples treated in pH 3 and 12 solutions for 24 h.

FTIR-DRIFT spectra of the surface of the  $\alpha$ -alumina sample, which was treated for 24 h in pH 3 and 12 solutions, are given in Fig. 10. It can be seen that the reflectance for the OH stretching region between wavelengths 2800 and 3800  $\text{cm}^{-1}$ , which corresponds to the H-bonded water, is deeper in the case of pH 12. Calculation of the areas in this region gives normalized areas of 1.00 for pH 12 and 0.67 for pH 3. This implies

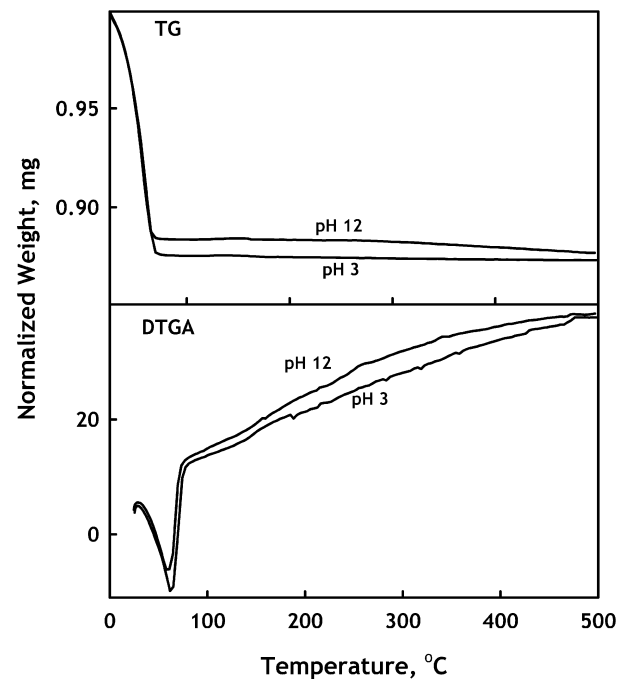


Fig. 11. TG and DTGA normalized data for the  $\alpha$ -alumina samples treated with pH 3 and 12 solutions for 24 h.

that the surface of alumina contains more H-bonded water in the case of basic pH. Raharjo et al. [41] observed surfaces of the different  $\alpha$ -alumina powders using FTIR-DRIFT analysis and molecular simulations.

TG and DTGA analysis of the same samples are given in Fig. 11. The figure shows that almost all the water was lost before 100 °C for the sample treated at pH 3, indicating that the water was physically adsorbed. The pH 12 sample, on the other hand, retained some amount of water to temperatures over 200 °C, indicating strong adsorption most probably in the form of H-bonded water. Staszczuk et al. [42] report the presence of chemisorbed water 1–2 layers thick that could only be removed from the surface at higher temperatures. Lefevre et al. [43] state that  $\gamma$ -alumina samples hydrated for 2 days show water loss at temperatures between 200 and 400 °C. All these results agree with Alwitt [44], who observed a dehydration peak for alumina between 280 and 330 °C.

## 5. Conclusions

AFM–colloid probe normal and lateral force measurements between  $\alpha$ - and  $\rho$ -alumina colloid probes and 0001 sapphire substrates were carried out within a wide pH range. The following conclusions could be made:

- (1) The normal force measurements and their comparison with the DLVO theory show that the interaction between aluminum oxide surfaces is solely governed by electrostatic and van der Waals forces at acidic pH values. A repulsive barrier and a primary minimum are clearly observable in the force curves and the DLVO theory describes this system extremely well.
- (2) For strongly basic solutions, the behavior of the alumina surfaces is profoundly different. The interaction is always repulsive, especially at separations below 5 nm, most probably due to the hydration of the oxide surface. The data suggest that the hydration layer acts as a repulsive barrier at separations closer than 10 nm. Therefore, the DLVO theory fails to represent the measured data at basic pH range.
- (3) The differences observed in the normal forces at acidic and basic pH values have a big influence on the lateral forces between the alumina surfaces. The frictional force between the two surfaces decreases precipitously where the hydration repulsion seems to be dominant. These findings have important implications in the stability, rheology, and forming behavior of the alumina powders, and very probably of the other metal oxide systems.

## Appendix A

Example *Mathematica* algorithm for numerical evaluation of the nonlinear Poisson–Boltzmann equation to calculate the potential profile between two dissimilar plates.

Line 1:  $H = 1$ ;  $S_l = -7.61$ ;  $S_u = 0.7$ ;  $Sinc = (S_u - S_l)/50/N$ ;  
*Defines the separation as  $H = 1$  and the shooting range for  $dY/dX$  on the first plate between lower  $S_l$  and upper  $S_u$  values.*

Line 2:  $fpend[S\_]: = f[H]/.NDSolve[{f''[Y] == Sinh[f[Y]], f[0] == 2.0, f'[0] == S}, f\{Y, 0, H\}]$

*Starts the shooting procedure by numerically solving the equation for each  $S$  value between  $S_l = -7.61$  and  $S_u = -0.7$  for an initial potential of  $Y = 2$  on the first plate.*

Line 3:  $Table\{S, fpend[S]\}, \{S, S_l, S_u, Sinc\}$

*Pairs the  $S$  estimates and the corresponding solutions together in a range.*

Line 4:  $fpS = Interpolation[\%]; fpS[S]$

*Obtains an interpolation of the above range and assigns it to a function.*

Line 5:  $lst2 = \{-20, -14, -10, -8, -5.7, -4, -2.8, -2, -1.4, -1, -0.8, -0.57, -0.4, -0.28, -0.2, -0.14, -0.1, -0.08, -0.057, -0.04, -0.028, -0.02, -0.014, -0.01, 0, 0.01, 0.014, 0.02, 0.028, 0.04, 0.057, 0.08, 0.1, 0.14, 0.2, 0.28, 0.4, 0.57, 0.8, 1, 1.4, 2, 2.8, 4, 5.7, 8, 10, 14, 20\}$

*Interpolation range for  $Y$ .*

Line 6:  $FindRoot[fpS[S] == -1.5, \{S\{S_l, S_u\}\}]$

*For  $Y_2 = -1.5$  finds the correct slope from the range in Line 5. The output, which is  $-4.073$  for this case, is the charge density  $S$  for  $Y_2 = 2$  and  $-1.5$ .*

Line 7:  $\{S = \{-4.073, -4.073\}\}$

Line 9:  $NDSolve\{f''[Y] = Sinh[f[Y]], f[0] == 2, f'[0] == -4.073\}, f\{Y, 0, H\}$

*This is the actual numerical solution line for initial values of  $Y_1 = 2$  and  $dY/dX = S = -4.073$ .*

Line 10:  $Plot[Evaluate[f[Y]/.\%], \{Y, 0, H\}, PlotRange \rightarrow All]$

*Plots the potential profile as a function of  $X$ . The algorithm outputs the  $Y_1, Y_2, S_1,$  and  $S_2$  values for a given  $H$ , which then can be employed to calculate the electrostatic pressure at that  $H$ .*

## References

- [1] D. Tabor, R.H.S. Winterton, Proc. R. Soc. A 312 (1969) 435.
- [2] J.N. Israelachvili, D. Tabor, Proc. R. Soc. A 331 (1972) 19.
- [3] J.N. Israelachvili, Acc. Chem. Res. 20 (1987) 415.
- [4] R.G. Horn, J.N. Israelachvili, F. Pribac, J. Colloid Interface Sci. 115 (1987) 480.
- [5] R.G. Horn, D.R. Clarke, M.T. Clarkson, J. Mat. Res. 3 (1988) 413.
- [6] T. Arai, M. Fujihira, J. Electroanal. Chem. 374 (1994) 269.
- [7] A. Ducker, T.J. Senden, R.M. Pashley, Nature 353 (1991) 239.
- [8] W.A. Ducker, T.J. Senden, R.M. Pashley, Langmuir 8 (1992) 1831.
- [9] W.A. Ducker, Z. Xu, D.R. Clarke, J.N. Israelachvili, J. Am. Ceram. Soc. 77 (1994) 437.
- [10] D.P.E. Smith, Rev. Sci. Instrum. 66 (5) (1995) 3191.
- [11] J.L. Parker, Prog. Surf. Sci. 47 (3) (1994) 205.
- [12] P.M. Claesson, T. Ederth, V. Bergeron, M.W. Rutland, Adv. Colloid Interface Sci. 67 (1996) 119.
- [13] T.J. Senden, Curr. Opin. Colloid Interface Sci. 6 (2001) 95.
- [14] C.S. Hodges, Adv. Colloid Interface Sci. 99 (2002) 13.
- [15] B.V. Derjaguin, L. Landau, Physicochim. URSS 14 (1941) 633.
- [16] E.J.W. Verwey, J.T.G. Overbeek, Theory and Stability of Lyophobic Colloids, Elsevier, Amsterdam, 1948.
- [17] R.J. Hunter, H.J.L. Wright, J. Colloid Interface Sci. 37 (1971) 564.
- [18] R.M. Pashley, J. Colloid Interface Sci. 83 (1981) 531.
- [19] B.V. Velamakanni, J.C. Chang, F.F. Lange, D.S. Pearson, Langmuir 6 (1990) 1323.
- [20] M.E. Karaman, R.M. Pashley, T.D. Waite, S.J. Hatch, H. Bustamante, Colloids Surf. A 129–130 (1997) 239.

- [21] L. Meagher, G.V. Franks, M.L. Gee, P.J. Scales, *Colloids Surf. A* 146 (1999) 123.
- [22] M. Manciu, E. Ruckenstein, *Adv. Colloid Interface Sci.* 112 (2004) 109.
- [23] S. Marcelja, *Curr. Opin. Colloid Interface Sci.* 9 (2004) 165.
- [24] A.V. Nguyen, J. Nalaskowski, J.D. Miller, H.J. Butt, *Int. J. Miner. Process.* 72 (2003) 215.
- [25] E.F. Teschke, E.F. de Souza, *Chem. Phys. Lett.* 403 (2005) 95.
- [26] T. Nagaoka, T. Tsugoshi, Y. Hotta, M. Yasuoka, K. Watari, *J. Ceram. Soc. Jpn.* 114 (2) (2006) 214.
- [27] G.V. Franks, L. Meagher, *Colloids Surf. A* 214 (2003) 99.
- [28] J.E. Sader, *J. Appl. Phys.* 84 (1998) 64.
- [29] J.E. Sader, *Rev. Sci. Instrum.* 70 (1999) 3967.
- [30] J.E. Sader, J.M.W. Chon, P. Mulvaney, *Rev. Sci. Instrum.* 70 (1999) 3967.
- [31] H. Polat, S. Chander, *Colloids Surf. A Physicochem. Eng. Aspects* 146 (1999) 199.
- [32] M. Löbbus, W. Vogelsperger, J. Sonnefeld, A. Seidel, *Langmuir* 14 (1998) 4386.
- [33] D. Wolff-Boenisch, S.R. Gislason, E.H. Oelkers, C.V. Putnis, *Geochim. Cosmochim. Acta* 68 (2004) 4843.
- [34] D.N. Furlong, P.A. Freeman, A.C.M. Lau, *J. Colloid Interface Sci.* 80 (1981) 20.
- [35] G. Böhme, H. Krupp, W. Schnabel, in: E. Drauglis (Ed.), *Molecular Processes at Solid Surfaces*, 1969, p. 611.
- [36] H. Krupp, W. Schanabel, G. Walter, *J. Colloid Interface Sci.* 39 (1972) 421.
- [37] D. Bargeman, F. van Voorst Vader, *J. Electroanal. Chem. Interface Electrochem.* 37 (1972) 45.
- [38] J. Visser, *Surface Colloids Sci.* 8 (1975) 3.
- [39] S. Bhattacharjee, M. Elimelech, *J. Colloid Interface Sci.* 193 (1997) 273.
- [40] S. Bhattacharjee, J. Chen, M. Elimelech, *Colloids Surf.* 165 (2000) 143.
- [41] P. Raharjo, C. Ishizaki, K. Ishizaki, *J. Ceram. Soc. Jpn.* 108 (5) (2000) 449.
- [42] P. Staszczuk, M. Jaroniec, R.K. Gilpin, *Anal. Chim. Acta* 269 (1992) 157.
- [43] G. Lefevre, M. Duc, P. Lepent, R. Caplain, M. Fedoroff, *Langmuir* 18 (2002) 7530.
- [44] R.S. Alwitt, in: J.W. Diggle, A.K. Wijn (Eds.), *Oxide and Oxide Films*, vol. 4, Dekker, New York, 1976, p. 169.